

Entanglement measures of Majorana bound states

Vimalesh Kumar Vimal and Jorge Cayao

Department of Physics and Astronomy, Uppsala University, Box 516, S-751 20 Uppsala, Sweden

(Dated: April 24, 2024)

Majorana bound states emerge in topological superconductors as zero-energy edge states exhibiting spatial nonlocality. Despite the enormous advances, the detection of Majorana bound states is still challenging mainly because topologically trivial Andreev bound states produce similar signatures. In this work we consider a topological superconductor with Majorana bound states coupled to quantum dots and investigate the dynamics of their quantum correlations with the aim to explore their entanglement properties. In particular, we characterize entanglement by using concurrence and discord, which are also complemented by the entanglement dynamics and return probability. We find that Majorana bound states at truly zero energy can transform an initially entangled system into its classical state, while they can create maximally entangled states at a finite energy overlap. Interestingly, we show that the system can generate a maximally entangled state between MBSs and a quantum dot by simply controlling the Majorana nonlocality. We demonstrate that these results hold in the scenarios when the initial state is either maximally entangled or separable, albeit in the latter maximally entangled states are achieved in the long time dynamics. Furthermore, we contrast our findings with those produced by a regular fermion and obtain very distinct entanglement signatures. Our work offers an alternative approach to characterize Majorana bound states, which can be also useful towards their utilization for quantum information tasks.

I. INTRODUCTION

Majorana bound states (MBSs) have become one of the central topics in condensed matter physics [1–9] largely due to their promising properties for fault tolerant quantum computation [10–14]. MBSs were initially predicted to appear in the topological phase of spinless p -wave superconductors, which later were shown to be realized by combining spin-orbit coupling, an external magnetic field, and conventional spin-singlet s -wave superconductivity, see e.g., Ref. [9]. MBSs emerge at zero-energy with their wavefunctions located at the system edges, thus exhibiting an inherent spatial nonlocality. In this regard, truly zero-energy MBSs are needed for realizing qubits that are robust against local perturbations [10]. However, zero-energy signatures can be also produced by trivial Andreev bound states [15–28], which proliferate in real devices and have challenged the detection of MBSs [7].

A less explored property of MBSs is their spatial nonlocality, which can be revealed by inducing a finite spatial overlap between Majorana wavefunctions [18, 29–31]. In this case, MBSs acquire a finite energy splitting, which, although not beneficial for realizing topological qubits, is useful for distinguishing the inherent Majorana nature. Following this idea, it has been recently shown that testing the Majorana nonlocality allows to distinguish between MBSs and trivial Andreev bound states [32–40]. Even though accessing the Majorana nonlocality might be difficult, it offers a solid way for the unambiguous detection of MBSs [34]. Moreover, since the spatial nonlocality reflects the MBSs at spatially separated regions, it is natural to wonder if such a spatial nonlocality carries quantum correlations and influences entanglement properties of the system.

In this work we consider a topological superconductor with two MBSs coupled to quantum dots (QDs) as

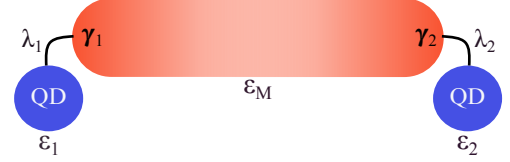


FIG. 1. Sketch of the studied system: a topological superconductor (red) hosting MBSs $\gamma_{1,2}$ is coupled by $\lambda_{1,2}$ to two QDs (blue) with onsite energies $\epsilon_{1,2}$. The spatial overlap between γ_1 and γ_2 originates and energy splitting represented by ϵ_M .

in Fig. 1 and investigate their entanglement properties. In particular, we characterize entanglement by exploring the dynamics of concurrence and discord, quantum correlations that we also complement by obtaining the entanglement dynamics and return probability. We find that zero-energy MBSs, which are completely localized at the edges, can evolve an initial state of maximally entangled QDs to a classical state of the system. Interestingly, we discover that a finite Majorana overlap enables maximally entangled states between MBSs and a QD, an effect that is fully controllable by the couplings to the QDs. We show that the entanglement generation occurs when the initial state is maximally entangled and, surprisingly, also for an initial separable state, where maximal entanglement in the latter is achieved in the long time dynamics. In both cases, the entanglement signatures are intimately tied to energy overlap between MBSs and, therefore, associated to their spatial nonlocality. We also show that QDs mediated by a regular fermion does not produce the entanglement signatures found for MBSs.

The paper is organised as follows: In Section II, we describe the model Hamiltonians of the systems and obtain their eigenspectrums. In Sec. III, we briefly de-

scribe the different measures of quantum correlations and state dynamical quantities. Following that, in Sec. IV, we compute the state dynamical functions and quantum correlation measures and give analytical expressions for all quantities for different initial states. Subsequently, we discuss the results in the later part of the section. Finally, in Section V, we summarise and conclude the results.

II. THE MODEL HAMILTONIANS AND METHODS

We are interested in exploring quantum correlations and entanglement signatures of MBSs. For this purpose, we consider a topological superconductor hosting MBSs and couple them to two QDs, as shown in Fig. 1. Moreover, we contrast this topological model by replacing the nonlocal fermion, arising due to both MBSs, with a regular fermion. In what follows we present these two models, discuss their properties, and introduce the methods used in this work to quantify entanglement measures.

A. QDs coupled through MBSs

The Hamiltonian describing the two MBSs coupled to QDs is given by

$$H = \frac{i\epsilon_M}{2}\gamma_1\gamma_2 + \sum_{j=1,2} \epsilon_j d_j^\dagger d_j + \lambda_j (d_j^\dagger - d_j)\gamma_j, \quad (1)$$

where γ_i represents a Majorana operator, ϵ_M is the energy of their splitting between MBSs, $d_j^\dagger(d_j)$ creates (annihilates) a fermionic state in the QDs, and λ_j characterizes the coupling between QDs MBSs. We note that the energy splitting ϵ_M reflects the Majorana nonlocality and can be approximated as $\epsilon_M \sim e^{-L/l}$, where L is the length of the topological superconductor and l is the Majorana localisation length.

To access quantum correlations and entanglement, it is convenient to write Eq. (1) in terms of fermionic operators and then handle it in a number represent basis. Thus, the two Majorana operators are transformed into a nonlocal fermion by using $\gamma_1 = i(f^\dagger - f)$, $\gamma_2 = f^\dagger + f$, where f represents the nonlocal fermion made of Majorana operators. Now, the two QDs plus the nonlocal fermion represent a three fermion system, with number operators $n_{d_i} = d_i^\dagger d_i$ for the QDs while $n_f = f^\dagger f$ for the nonlocal fermion operator. This allows us to define a three qubit system which will be analyzed next.

Before going further, we adopt some simplifications that will allow us to derive analytical expressions. The on-site energies of the QDs are set to zero $\epsilon_{d_1} = \epsilon_{d_2} = 0$, the coupling to the left QD is set to unity $\lambda_1 = 1$, $\omega = \epsilon_M/2$, $\lambda_2 = \lambda$, and $\hbar = 1$. Hence, tuning λ and ω allow us to control the properties of the entire system. We now proceed to write Eq. (1) in the number representation basis defined by $|n_{d_1}, n_{d_2}, n_f\rangle$. In this regard,

we note that, since the Hamiltonian commutes with the fermion parity operator $(-1)^N$, with N being the total number of fermions, the odd and the even sectors do not mix and can be solved separately. We focus on the even sector with basis states $|000\rangle$, $|011\rangle$, $|101\rangle$, and $|110\rangle$. The even Hamiltonian can be then written as,

$$H_e = \begin{pmatrix} -\omega & \lambda & -1 & 0 \\ \lambda & \omega & 0 & -1 \\ -1 & 0 & \omega & \lambda \\ 0 & -1 & \lambda & -\omega \end{pmatrix}. \quad (2)$$

The eigenvalues of the even sector are then given by

$$E_i = \pm \sqrt{(\lambda \pm 1)^2 + \omega^2}, \quad (3)$$

where $E_{1(2)} = \mp\Delta$ and $E_{3(4)} = \mp\Delta_1$, with $\Delta = \sqrt{(\lambda - 1)^2 + \omega^2}$ and $\Delta_1 = \sqrt{(\lambda + 1)^2 + \omega^2}$. The eigenvectors $|E_j\rangle$ in increasing value of j can be written as un-normalized column vectors in the order of its corresponding eigenvalues as

$$EV = (|E_1\rangle |E_2\rangle |E_3\rangle |E_4\rangle), \quad (4)$$

where $|E_1\rangle = (1, (\omega - \Delta)/(\lambda - 1), (\omega - \Delta)/(\lambda - 1), 1)^T$ and T is the transpose operation. Moreover, $|E_2\rangle = |E_1(\delta \rightarrow -\delta)\rangle$, $|E_{3(4)}\rangle = |E_{1(2)}(\Delta \rightarrow \Delta_1)\rangle$. We note that all the eigenvalues in Eqs. (3) have contributions from both λ and ω , while the respective eigenstates in Eq. (4) exhibit contributions from all configurations in the even ket states listed above Eq. (2). This distribution of the Hamiltonian parameters in the eigenvalues and eigenvectors arises precisely from the nonlocal fermionic structure of MBSs.

B. QDs coupled through a normal fermion

To contrast our results, here we discuss a model where the QDs are coupled via a normal fermion, which is not nonlocal and therefore of no Majorana origin. We model this normal fermion system (NFS) by the following Hamiltonian,

$$H_{\text{NFS}} = \epsilon_c c^\dagger c + \sum_j \epsilon_j d_j^\dagger d_j + \lambda_j (d_j^\dagger c + h.c.), \quad (5)$$

where ϵ_c is onsite fermion energy, $c^\dagger(c)$ creation (annihilation) operators of the normal fermion, while $d_i^\dagger(d_i)$ is the creation (annihilation) operator in the QDs. Here, the coupling between QDs and the normal fermion is characterized by λ_j . We set $\epsilon_c = 2\omega$ so that we treat the energies of the nonlocal and regular fermion in Eqs. (1) and Eq. (5) at the same level. As for the Majorana system, we solve Eq. (5) in the even sector spanned by number operator basis states, $|n_{d_1} n_{d_2} n_c\rangle$ and consider the same energy unit $\lambda_1 = 1$ so that the coupling to the right QD is $\lambda_2 = \lambda$. We then obtain the eigenvalues which for the even sector are given by

$$E'_i = \{0, 2\omega, \Delta_-, \Delta_+\}, \quad (6)$$

where $\Delta_{\pm} = \omega \pm \sqrt{1 + \lambda^2 + \omega^2}$. Moreover, the associated unnormalized eigenstates for increasing values of i in E'_i are given by

$$EV_{\text{NFS}} = (|E'_1\rangle | |E'_2\rangle | |E'_3\rangle | |E'_4\rangle), \quad (7)$$

where $|E'_1\rangle = (1, 0, 0, 0)^T$, $|E'_2\rangle = (0, \lambda, 1, 0)^T$, $|E'_3\rangle = (0, 1/\Delta_+, -\lambda/\Delta_+, 1)^T$, and $|E'_4\rangle = (0, 1/\Delta_-, -\lambda/\Delta_-, 1)^T$. Before going further, it is worth pointing out that the first eigenvalue is zero with eigenstate $|E'_1\rangle$, which implies that it has only the configuration $|000\rangle$ where no excitations are present. In this first state, neither the onsite energy nor the hopping terms of the Hamiltonian contribute to the energy, resulting in a zero eigenvalue. The second eigenvalue solely depends on the energy associated with the normal fermion $\epsilon_c = 2\omega$, indicating the presence of the normal fermion in its eigenstate $|E'_2\rangle$ by having $|011\rangle$ and $|101\rangle$ terms but not $|000\rangle$ and $|110\rangle$. The last two eigenvalues depend on the parameters of the Hamiltonian and acquire eigenstates having mixtures of all possible excitations, except $|000\rangle$. This point is of interest because if $|000\rangle$ is not present in the initial state, it will not emerge throughout the dynamics, as we will show later.

C. Methods to quantify entanglement and the state dynamics

We are interested in exploring the effect of nonlocality on entanglement and quantum correlations in the systems discussed in previous section. To address this task, we focus on bipartite subsystems described by a reduced density matrix ρ_d obtained as [41]

$$\rho_d = \text{Tr}_{d'}(\rho), \quad (8)$$

where ρ is the density matrix of the composite three qubit system, $\text{Tr}_{d'}$ represents the partial trace operation over a subsystem such that ρ_d describes a two qubit system. We remind that the three qubit system is formed by the two QDs and either the nonlocal fermion due to MBSs or a normal fermion, see Section II for more details on the models. The density matrix in Eq. (8) is obtained by using a standard approach $\rho = |\psi\rangle\langle\psi|$, where $|\psi\rangle$ corresponds to the state of the system [41]. We anticipate that, because we are interested in the dynamical properties, we use the time-evolved states of the Majorana and normal fermion systems discussed in previous section, taking into account different initial states in both systems. Then, all the bipartite quantum correlations can be studied by calculating the reduced density matrix ρ_d given by Eq. (8), thus providing a starting point for exploring various entanglement measures. In particular, we will address the concurrence and discord because they provide a unify way to quantify entanglement and quantum correlations [41]. To complement these quantities, we will also address the state dynamics by employing the

return probability and the entanglement dynamics. To make this work self contained, in what follows we briefly describe the fundamental aspects of these quantities.

1. Concurrence

The concurrence, denoted here by C , measures entanglement between two qubits in a mixed state [42]. The concurrence is calculated as [42]

$$C = \max(\lambda_1 - \lambda_2 - \lambda_3 - \lambda_4, 0), \quad (9)$$

which correspond to the maximum of the eigenvalues λ_i , with them being the eigenvalues in decreasing order of the matrix $R = \sqrt{\sqrt{\rho_d}\tilde{\rho}_d\sqrt{\rho_d}}$. The matrix $\tilde{\rho}_d$ is defined as $\tilde{\rho}_d = \sigma_y \otimes \sigma_y \rho_d^* \sigma_y \otimes \sigma_y$, where ρ_d^* is the complex conjugate reduced density matrix ρ_d given by Eq. (8). In our systems, the reduced density matrices in the basis states of $|00\rangle$, $|01\rangle$, $|10\rangle$, and $|11\rangle$ acquire the following form

$$\rho_d = \begin{pmatrix} u & 0 & 0 & y^* \\ 0 & w_1 & x^* & 0 \\ 0 & x & w_2 & 0 \\ y & 0 & 0 & v \end{pmatrix}, \quad (10)$$

which takes the form of a X -state because the subsystems are in even sectors, and the odd and even sectors do not mix within the system [43]. We note that the non-zero matrix elements in Eq. (10) represent correlation functions between the two qubits, which, as we will see in the next section, turn out to be functions of the coefficients of the eigenfunctions. The zero elements represent the fact that the odd and even states do not mix in the system. For the reduced density matrix by Eq. (10), the concurrence can be written as

$$C = 2 \max(|x| - \sqrt{uv}, |y| - \sqrt{w_1 w_2}, 0). \quad (11)$$

Before going further, a few comments are in order at this stage. The concurrence given by Eq. (11) remains finite if the off-diagonal correlation functions (x, y) dominate over their diagonal counterparts $(\sqrt{uv}, \sqrt{w_1 w_2})$; otherwise, C goes to zero. A zero concurrence $C = 0$ signals that appearance of an unentangled state of the system but, importantly, this does not imply that the total quantum correlations in the system are completely lost or absent [44]. The approach discussed here will be used later to obtain the concurrence and investigate entanglement in a bipartite system.

2. Quantum discord

To quantify quantum correlations beyond entanglement, we focus on the quantum discord because it measures purely quantum correlations in a bipartite system. The quantum discord is of particular relevance when exploring the dynamics of the system, which, although acquiring a non-entangled state at certain times, may still

exhibit finite quantum correlations [45–52]. The discord is a bipartite correlation measure, and, in this sense, it is similar to concurrence. It is defined by the difference between two classically equivalent expressions of the total correlation, characterized by the quantum mutual information [53]. It is thus useful to first introduce the quantum mutual information, which, for subsystems A and B, is characterized by [53]

$$\begin{aligned} I(\rho_{AB}) &= S(\rho_A) + S(\rho_B) - S(\rho_{AB}), \\ J(\rho_{AB}) &= S(\rho_A) - C_{\theta, \phi}(\rho_{A|B}), \end{aligned} \quad (12)$$

where $S(\rho)$ is the entropy associated to ρ and calculated as $S(\rho) = -\text{Tr}(\rho \log_2 \rho)$, while $C_{\theta, \phi}(\rho_{A|B})$ is the conditional entropy of A given the state of B. Moreover, $\rho_{A(B)}$ is the reduced density matrix of A(B), ρ_{AB} is the composite reduced density matrix of the subsystem AB, and $\rho_{A|B}$ represents the conditional density matrix. Furthermore, the conditional entropy is obtained as [53]

$$C_{\theta, \phi}(\rho_{A|B}) = \min_{\{B_{\tilde{\kappa}}\}} \sum_{\tilde{\kappa}} p_{\tilde{\kappa}} S(\rho_{A|B_{\tilde{\kappa}}}), \quad (13)$$

where θ and ϕ are angles that parametrize the measurement basis of B, $\{B_{\tilde{\kappa}}\} = \{|\tilde{\kappa}\rangle\langle\tilde{\kappa}|\}$ is a complete set of projection operators corresponding to local measurements on B, and min indicates that a minimization operation with respect to $\{B_{\tilde{\kappa}}\}$ is carried out to find C . Also, $p_{\tilde{\kappa}}$ on the right hand side of Eq. (13) denotes the probability of measurement outcome $\tilde{\kappa}$ and is defined as $p_{\tilde{\kappa}} = \text{Tr}[(\sigma_0 \otimes B_{\tilde{\kappa}})\rho_{AB}(\sigma_0 \otimes B_{\tilde{\kappa}})]$, with σ_0 representing the identity matrix for A. Moreover, $\rho_{\tilde{\kappa}} = (\sigma_0 \otimes B_{\tilde{\kappa}})\rho_{AB}(\sigma_0 \otimes B_{\tilde{\kappa}})/p_{\tilde{\kappa}}$, which represents that it is the density matrix ρ_{AB} conditioned to the measurement outcomes $\tilde{\kappa}$ and weighted over different outcomes of marginal conditional entropies $S(\rho_{A|B_{\tilde{\kappa}}})$. The term $\rho_{A|B_{\tilde{\kappa}}}$ represents the conditional density matrices in the $|\tilde{\kappa}\rangle$ basis. In terms of all the above considerations, the quantum discord is defined as [53]

$$D_{AB} = \min[I(\rho_{AB}) - J(\rho_{AB})]. \quad (14)$$

where $I(\rho_{AB})$ and $J(\rho_{AB})$ are given by Eqs. (12). The minimization of the conditional entropy makes the quantum discord a quantifier of truly quantum correlation. In Appendix A, we provide step-by-step calculations of discord in different subsections for both MS and NFS.

3. State dynamics

One of the basic interests in quantum systems is to study the decay or revival of the initial state in the dynamics of the system. However, the state dynamics can also be manipulated to understand the entanglement signatures of the subsystems over time. Motivated by these ideas, in this work we also address the dynamics of a maximally entangled state, called *entanglement dynam-*

ics and denoted by E_d , and the return probability denoted by R_p . These two quantities are obtained as

$$\begin{aligned} R_p &= |\langle\psi(0)|e^{-iHt}|\psi(0)\rangle|^2, \\ E_d &= |\langle\phi|e^{-iHt}|\psi(0)\rangle|^2. \end{aligned} \quad (15)$$

As we observe, the return probability R_p is defined by overlapping a time-evolved state with its initial state, while the entanglement dynamics E_d is defined by projecting a time-evolved state function onto a desired state $|\phi\rangle$, whose explicit form will be given later. It is worth noting that, due to the definitions in Eqs. (15), the return probability always begins with unity, regardless of the chosen initial states. However, the initial value for the entanglement dynamics depends on both the initial and the desired states. With Eqs. (15) as well as with those for concurrence and discord, we are now in position to explore the quantum correlations and entanglement signatures for the subsystems discussed in Section II.

III. RESULTS FOR A MAXIMALLY ENTANGLED INITIAL STATE

In this part, we follow the discussion of previous section and obtain the quantum correlations and state dynamic probabilities for the two systems described in Section II, taking into account a maximally entangled initial state. We remind that the first introduced setup corresponds to a Majorana system (MS), where QDs are coupled via nonlocal fermion of Majorana origin. The second setup consists of QDs coupled via a normal fermion, coined normal fermion system (NFS). Since the manipulation of QDs was shown to be a feasible task [54, 55], see also Refs. [56–58], we consider that the two QDs are in a maximally entangled initial state, while the nonlocal fermion due to MBSs is in the zero state. We note that it is necessary to consider the zero state of the nonlocal fermion in order to maintain the even parity of the system, which is the sector we investigate, see Section II. The separability of the non-local fermion with entangled QDs is justified by assuming that the topological superconductor and QD are not coupled before the evolution of the entire system starts.

The initial state can be thus written as

$$|\psi(0)\rangle = \frac{1}{\sqrt{2}}[|000\rangle + |110\rangle] = \left[\frac{|00\rangle + |11\rangle}{\sqrt{2}} \right] |0\rangle, \quad (16)$$

which corresponds to one of the Bell's states for the two QDs signalling that they are maximally entangled. The dynamics of the other maximally entangled states can be calculated in a similar fashion. We anticipate that the Bell's state $(|00\rangle - |11\rangle)/\sqrt{2}$ emerges in the dynamics, while the other two Bell's states are prohibited by the parity of the system. Then, the state function for the initial state given in Eq. (16) is obtained as

$$|\psi(t)\rangle = e^{-iHt}|\psi(0)\rangle = \sum_j^4 e^{-iE_j t} |E_j\rangle \langle E_j|\psi(0)\rangle, \quad (17)$$

where $|E_j\rangle$ represents the eigenstates of the MS or NFS ($|E_j\rangle \rightarrow |E'_j\rangle$) given by Eqs. (4) or Eqs. (7), depending on the system under investigation. Before going further, we point out that the contribution from the eigenstates in Eq. (17) also depends on the form of the initial states. In this regard, we have that the primary contributions in the MS come from eigenstates $|E_1\rangle$ and $|E_2\rangle$ with energies $-\Delta$ and Δ , respectively. The eigenstates $|E_3\rangle$ and $|E_4\rangle$ are orthogonal to the initial state, $\langle E_j|\psi(0)\rangle = 0$, which implies that they do not contribute to the dynamics given by Eq. (17). Contrary to the MS, the dynamics of the NFS is given by the contribution of all states.

A. Majorana system

In the case of the system with MBSs, the time-evolved state given by Eq. (17) acquires the form given by

$$\begin{aligned} |\psi(t)\rangle = & \frac{1}{\sqrt{2}} |0\rangle (\eta |00\rangle + \chi |11\rangle) \\ & + \frac{1}{\sqrt{2}} |1\rangle (\eta |10\rangle + \chi |01\rangle), \end{aligned} \quad (18)$$

where χ and η are time-dependent and given by

$$\begin{aligned} \eta(t) &= \frac{1}{\Delta} (\Delta \cos \Delta t + i\omega \sin \Delta t), \\ \chi(t) &= \frac{-i}{\Delta} (\lambda - 1) \sin \Delta t. \end{aligned} \quad (19)$$

Here, Δ , λ , and ω is the lowest positive eigenvalue, the coupling between nonlocal fermion and right QD, and the energy splitting between MBSs, see Subsection 4. The coefficients η and χ in the above state function shape the dynamics of the entanglement generations between the MBSs and the second QD. They can also be manipulated to see the type of maximally entangled state (of the Bell's state form) that may be achieved in the evolution. Therefore, below we now compute the quantities discussed in Section II C.

1. Return probability and entanglement dynamics

By using Eqs. (15), we obtain the entanglement dynamics E_d and the return probability R_p . For E_d we need to specify the desired state onto which will be projected the time-evolved function $|\psi(t)\rangle$. For this purpose, we consider $|\phi\rangle$ describing a maximally entangled nonlocal fermion and the second QD given by

$$|\phi\rangle = \frac{1}{\sqrt{2}} [|000\rangle + |011\rangle] = |0\rangle \frac{1}{\sqrt{2}} (|00\rangle + |11\rangle), \quad (20)$$

where the second equality expresses the essence of the considered maximal entanglement. Then, using Eqs. (15), along with Eq. (17), Eq. (16), and Eq. (20), we

find that the return probability and entanglement dynamics are given by

$$\begin{aligned} R_p &= |\eta|^2, \\ E_d &= \left| \frac{\eta + \chi}{2} \right|^2, \end{aligned} \quad (21)$$

where η and χ correspond to the time-dependent coefficients of the time-evolved state and given by Eqs. (19). Interestingly, we see that the entanglement dynamics E_d is sensitive to the local phases in the state function, unlike the return probability. This sensitivity is crucial for visualizing other maximally entangled states generated during the evolution.

2. Concurrence

We are interested in computing the concurrence between the two QDs for the initial state written in Eq. (16). For this purpose, we follow the recipe discussed in Subsection II C 1, which involves obtaining the density matrix elements associated to the time-evolved state Eq. (18) and then using Eq. (11). We obtain the density matrix and find that its elements are given by $u = v = y = |\eta|^2/2$, $w_1 = w_2 = x = |\chi|^2/2$. Therefore, using Eq. (11), we find that the concurrence is given by

$$C = ||\eta|^2 - |\chi|^2|, \quad (22)$$

where the modulus in the expression on the right-hand side arises from the fact that particular sets of diagonal and off-diagonal elements of the density matrix have the same expression. From Eq. (22), we identify that the concurrence vanishes with $C = 0$ only when $|\eta| = |\chi|$. It is worth noting that zero concurrence has many properties, including the signature of entanglement monogamy [59], which states that the entanglement cannot be freely shared between more than two parties. We will provide a deeper analysis of the zero concurrence regime by comparing it with the entanglement dynamics and the return probability later in this section.

3. Quantum discord

To compute quantum discord in MS, we follow the discussion provided in Subsection II C 2 along with Eq. (14) to obtain the discord between the two QDs represented by A and B. Detailed calculations are carried out in the first subsection of Appendix A, formulating the quantum discord as follows:

$$D_{AB} = \min_{(\theta, \phi)} C_{\theta, \phi}(\rho_{A|B}) - S(\rho_{AB}) + S(\rho_B), \quad (23)$$

where the term $C_{\theta, \phi}(\rho_{A|B})$ represents the conditional entropy of the first QD when the measurement basis of the second QD is parameterized by angles θ and ϕ . The term S_{AB} denotes the composite entropy of the two QDs, while S_B is the single-qubit entropy of the second QD. Further details of the calculation is given in Appendix A.

B. Normal fermion system

In this part we carry out the same calculations as in the previous subsection but when the QDs are coupled via a normal fermion. The time-evolved state function for the initial state from Eq. (16) is here given by

$$|\psi(t)\rangle = \bar{c}_1 |000\rangle + \bar{c}_2 |011\rangle + \bar{c}_3 |101\rangle + \bar{c}_4 |110\rangle, \quad (24)$$

where \bar{c}_i are time-dependent coefficients given by

$$\begin{aligned} \bar{c}_1(t) &= \frac{1}{\sqrt{2}}, \\ \bar{c}_2(t) &= \frac{1}{2\sqrt{2(1+\lambda^2+\omega^2)}}(e^{-i\Delta-t} - e^{-i\Delta+t}), \\ \bar{c}_3(t) &= \frac{-\lambda}{2\sqrt{2(1+\lambda^2+\omega^2)}}(e^{-i\Delta-t} - e^{-i\Delta+t}), \\ \bar{c}_4(t) &= \frac{1}{2\sqrt{2(1+\lambda^2+\omega^2)}}(\Delta_+ e^{-i\Delta-t} - \Delta_- e^{-i\Delta+t}). \end{aligned} \quad (25)$$

Hence, having all the coefficients finite implies that $|\psi(t)\rangle$ for the NFS has a general and complex structure, which makes it difficult to simplify the expressions of the entanglement measures in the system, unlike what we found for the MS in the subsection III A. Then, we find that the return probability, entanglement dynamics, and concurrence are given by

$$\begin{aligned} R_p &= \frac{|\bar{c}_1(t) + \bar{c}_4(t)|^2}{2}, \\ E_d &= \frac{|\bar{c}_1(t) + \bar{c}_2(t)|^2}{2}, \\ C &= 2 \max(|\bar{c}_1(t)||\bar{c}_4(t)| - |\bar{c}_2(t)||\bar{c}_3(t)|), \end{aligned} \quad (26)$$

while the discord acquires a more complicated form, whose details are discussed in Appendix A 2. We note that to calculate E_d , we consider Eq. (20) as the desired state onto which the time-evolved state Eq. (24) was projected. For the NFS, Eq. (20) has a slightly different meaning because the last qubit represents the normal fermion instead of the nonlocal fermion due to MBSs. Moreover, to find R_p , the initial state is taken as in Eq. (16). These considerations facilitate the comparison of NFS with MS. Even though the expressions in Eq. (26) acquire a complex form since \bar{c}_i are not simple at all, we will point out their simplification in special cases during the discussion of our results.

C. Discussion of the state dynamics and quantum correlations

Having presented the general expressions obtained of concurrence (C), discord (D), entanglement dynamics (E_d) and return probability (R_p) for the MS and the NFS with maximally entangled QDs, here we discuss

their time evolution. To visualize the time evolution, in Fig. 2 we plot C, D, E_d , and R_p as a function of time t for the two systems under consideration (MS and NFS). Fig. 2(a-d) and Fig. 2(e-h) correspond to QDs with symmetric ($\lambda = 1$) and asymmetric ($\lambda \neq 1$) couplings in the MS or NFS. As discussed before, in the MS setup QDs are coupled via MBSs, while QDs are coupled via a normal fermion in the NFS. To truly exploit the inherent Majorana nonlocality, in Fig. 2 we contrast regimes at zero and finite energies.

We first analyze the case of symmetric couplings and at zero energy, which corresponds to $\omega = 0$ and $\lambda = 1$ in Fig. 2(a,b). In the case of the MS, this regime has zero-energy MBSs and the first feature to notice is that the quantities C , D , and R_p remain at 1, while $E_d = 0.25$, as shown in Fig. 2(a), see also subsection III A. Since the initial state involves maximally entangled QDs, having a constant time evolution reveals that such a maximal entanglement is not affected. The constant time evolution can be understood by noting that the eigenstates of the Hamiltonian given by Eq. (4), except for the third eigenstate, are orthonormal to the initial state given by Eq. (17), giving a vanishing overlap that does not contribute to the dynamics as seen in Fig. 2(a). The third eigenstate of the MS is the same as the initial state [Eq. (16)] and has zero energy [Eq. (3)], implying that neither the quantities nor the state evolve at all.

In contrast to the MS setup, the quantum correlations and state dynamics for the NFS case exhibit an oscillatory behaviour with time, which start from unity reflecting the initial maximally entangled QDs, see Fig. 2(b). The distinct time evolution occurs because the contributing eigenvalues in Eq. (7) are finite for the NFS, implying that all the coefficients from Eqs. (25) contribute to the time evolution that becomes oscillatory over time. As time progresses, we observe that there are times where $C = 0$ but $D \neq 0$, signalling that there is a finite quantum correlation between the two QDs even when the NFS reaches its separable state whose specific form is not evident. Also, Fig. 2(b) shows that there are other times t at which $C = 1$ and $D = 1$ when $R_p = 0$, a regime showing that additional maximally entangled states of the QDs are being generated during the dynamics in the NFS [60]. For the return probability and entanglement dynamics of the NFS, their oscillatory behaviour can be easily seen analytically from Eqs. (26): $R_p = |(1 + \cos \sqrt{2}t)/2|^2$ with period $T = ((2n+1)\pi/\sqrt{2})\hbar/\lambda_1$, being n an integer and \hbar/λ_1 the unit of time, while $E_d = |(1 + i\sqrt{2}\sin \sqrt{2}t)/2|^2$ with period $T = (\pi/\sqrt{2})\hbar/\lambda_1$. It is straightforward to get $R_p = 1$ and $E_d = 1/4$ at $t = 0$, while at $t = (n\pi/\sqrt{2})\hbar/\lambda_1$ we get $R_p = 0$ and E_d develops minima leading to a fall of the state into the eigenstate $|000\rangle$, see by green and black curves in Fig. 2(b). The overall behaviour of the entanglement measures in the NFS setup is clearly different to what we found for the MS system. Therefore, zero-energy MBSs and zero-energy regular normal fermions induce distinct entanglement signatures

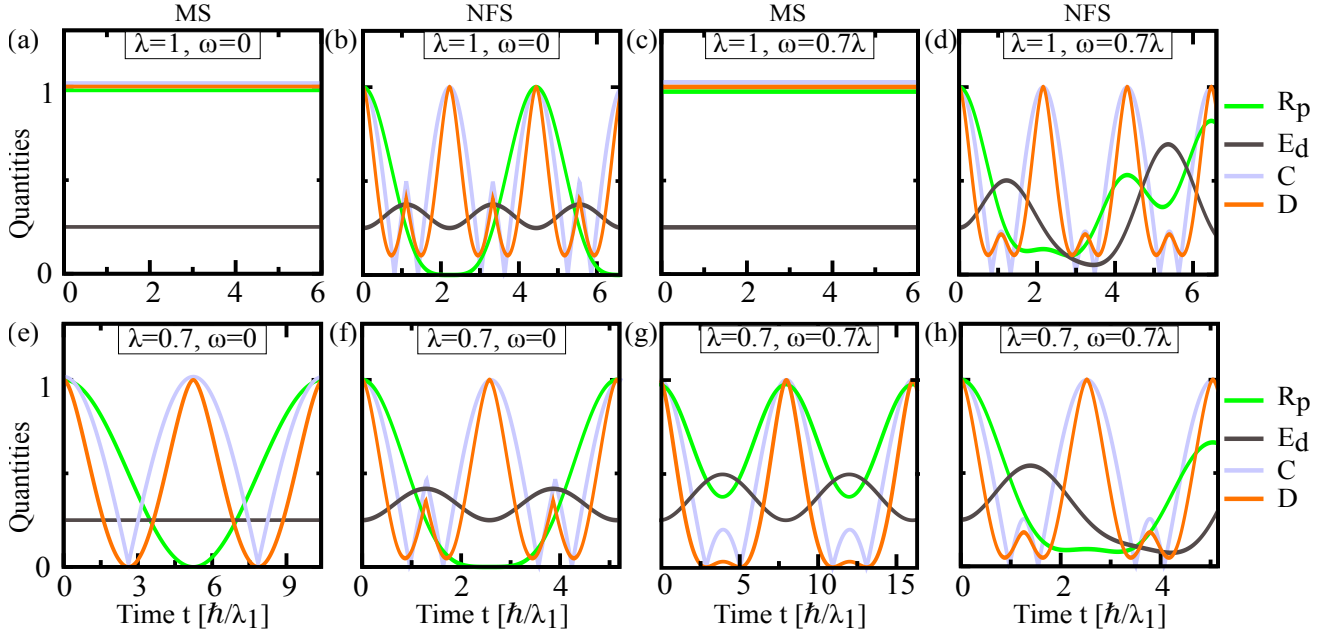


FIG. 2. Time evolution of concurrence, discord, return probability, and entanglement dynamics, denoted by C , D , R_p , and E_d , with an initial state of maximally entangled QDs for MS and NFS. Top row corresponds to a symmetric coupling to the left and right QDs $\lambda = 1$, with MBSs and normal fermion having zero energy $\omega = 0$ in (a,b), while MBSs and normal fermion having finite energy $\omega \neq 0$ in (c,d). Bottom row shows the same as in top row but for left and right QDs having asymmetric couplings to MBSs and normal fermion, namely, $\lambda \neq 1$.

In the case of finite energies $\omega \neq 0$ at symmetric couplings $\lambda = 1$, the time evolution of the entanglement measures exhibit a rather similar behaviour as the one for zero energy discussed in the previous two paragraphs, see Fig. 2(c,d). For the MS in Fig. 2(c), we find R_d , C , and D exhibiting a constant value equal to 1, while $E_d = 0.25$, which is the same to what we saw in Fig. 2(a) at $\omega = 0$. To understand the intriguing behaviour at $\omega \neq 0$, we note that the coefficient χ [Eq. (19)] of the time evolved state given by Eq. (18) vanishes at $\lambda = 1$ while the other coefficient becomes $\eta(t) = \cos(|\omega|t) + i\sin(|\omega|t)$ and is thus entirely determined by the energy splitting of MBSs. As a result, the time-evolved state from Eq. (18) evolves with a constant phase, determined by ω , where $|\eta(t)|^2 = 1$ enables C , D , and R_p to remain constant at 1 and $E_d = 0.25$, see Eq. (19). The quantities equal to 1 then imply that the system remains with maximally entangled QDs and $E_d = 0.25$ that there is only a contribution from the $|000\rangle$ configuration in the entanglement dynamics. For the NFS at $\lambda = 1$ and $\omega \neq 0$ in Fig. 2(d), the entanglement measures exhibit a time evolution that is similar to the $\omega = 0$ case but with some subtle differences. At $\omega \neq 0$, the periodic C and D develop maxima, which, however, are not accompanied by $R_p = 0$, implying that there is no revival of the initial state at short times [61]. This situation implies that another entangled state, having a component of the initial state, is being generated during the evolution. Moreover, the minima of E_d states that one of the configurations in $|\phi\rangle$ remains in the state function throughout the dynamics.

When the couplings become asymmetric $\lambda \neq 1$, the entanglement measures of the MS as well as those of the NFS develop an oscillatory profile, see Fig. 2(e-h). At $\omega = 0$, the MS with zero-energy MBSs achieves $D = 0$ and $C = 0$ at certain times, which is contrary to the NFS case, where $D \neq 0$ when $C = 0$, see Fig. 2(e,f). Besides this point, we also note that in the MS system the concurrence and discord reach unity when $R_p = 0$, showing another state, $(|000\rangle - |110\rangle)/\sqrt{2}$, of two maximally entangled QDs has been created. Moreover, the entanglement dynamics for the MS remains constant because the initial state changes only to $(|000\rangle - |110\rangle)/\sqrt{2}$, and then it revives back, resulting in a constant value of $E_d = 0.25$, while it oscillates for the NFS, again contrasting the distinct signatures of both systems [Fig. 2(e,f)]. At finite energies ($\omega \neq 0$) and asymmetric couplings ($\lambda \neq 1$), the MS and the NFS exhibit similar properties as seen in Fig. 2(g,h) but still with some small differences. The similar behavior is associated to the oscillatory profile which stems from having extra configurations participating in the dynamics because the coefficient of the time-evolved state in Eq. (19) is non zero, $\chi \neq 0$. It is worth noting that the entanglement measures for the MS setup have larger periodicity [Fig. 2(g)], which occurs because the eigenenergies in Eq. (4) have contributions from λ and ω , see also Eqs. (19) and Eq. (18). Among the differences at $\omega \neq 0$ and $\lambda \neq 1$, we find that the Majorana system MS achieves regimes with C , D , and R_p equal to 1 (as shown in Fig. 2(g)), which means that the finite ω prefers the revival of the initial state rather than

changing the local phase, which would result in achieving another maximally entangled state of quantum dots, as depicted for the MS in Fig. 2(e). This phenomenon, however, is not observed in the NFS, as shown in Fig. 2(h). Another difference is that in the NFS case, the quantities E_d and R_p exhibit a fall that reveal the presence of arbitrary configurations in the state; their peaks show that the different entangled states between the two QDs are being generated and destroyed. Thus, even though the oscillatory profile of the entanglement measures for the MS and NFS exhibit some similarities, there still are significant differences that could allow identifying MBSs.

Before closing this part, we highlight that the periodic characteristic of the state dynamics suggests the possible generation of maximally entangled states. Since we consider an initial state of maximally entangled QDs, it is natural to ask whether it is possible to generate maximal entanglement between other parts of the system, such as between MBSs and QDs. We address this question in the next subsection.

D. Generating a maximally entangled state between MBSs and a QD

As pointed out before, the oscillatory behaviour of the entanglement measures as functions of time imply a possible generation of maximally entangled states. Since the considered systems are composed of three subsystems (qubits), with an initial state of maximally entangled QDs, we focus on achieving a maximally entangled state between MBSs and the right QD. To find a maximally entangled state, it is necessary to have $\eta = \chi$ in Eq. (19), because this conditions places the time-evolved state given by Eq. (18) in the form of two qubit Bell's states, which are maximally entangled states [41]. Thus, taking this condition into account, we find the required parameters for achieving maximal entanglement. Then, we can choose $t = ((2n+1)\pi/2\Delta) \hbar/\lambda_1$ so that η is purely imaginary; then, by comparing the imaginary parts of χ and η , we find that they are equal when $\omega = 1 - \lambda$, which, using the expression for Δ below Eq. (3), gives $\Delta = \sqrt{2}|1 - \lambda|$. Under these conditions, we obtain $\eta = \chi = 1/\sqrt{2}$, which is expected to lead to a maximally entangled state between MBSs and QDs because, as we explained above, the time-evolved state acquires the form of two-qubit Bell states.

In spite of the seemingly stringent conditions to achieve maximally entanglement during the evolution, in Fig. 3 we show that it is possible at $\omega = 1 - \lambda$ and $\lambda = 0.7$ by plotting the time evolution of R_p , E_d , C , and D for the MS and NFS setups. Apart from the already seen oscillatory behaviour, there are two points we would like to highlight, which are marked by red and magenta stars in Fig. 3(a) for the MS setup. First, at the beginning of the evolution $t = 0$, we have $R_p = 1$, $C = 1$, $D = 1$, and $E_d = 0.25$, a regime that corresponds to the maximally entangled QDs. Second, at times given

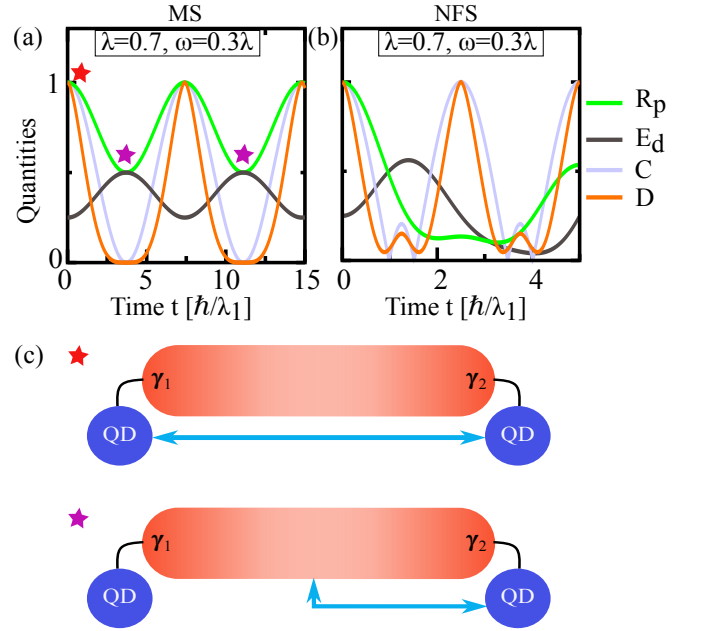


FIG. 3. Generation of a maximally entangled state between MBSs with a QD. (a,b) Time evolution of concurrence, discord, return probability, and entanglement dynamics, denoted by C , D , R_p , and E_d , with an initial state of maximally entangled QDs for MS and NFS. Here, $\lambda = 0.7$ and $\omega = 1 - \lambda$ in panels (a,b). The red star in (a) shows that the QDs are maximally entangled at the beginning of the evolution $t = 0$, whereas the magenta stars show that maximally entanglement between MBSs and the second QD is achieved at later times. (c) Schematic representation of the entangled systems indicated by red and magenta stars in (a), with the thick cyan arrow showing the entangled parts. The NFS does not have this characteristic.

by $t = \pi/2\Delta = 3.7 \hbar/\lambda_1$, the entanglement dynamics and return probability become $E_d = 0.5$ and $R_p = 0.5$, implying the creation of a maximally entangled state of MBSs and the second QD, see magenta star in Fig. 3(a). This maximal entanglement is further confirmed by getting vanishing concurrence $C = 0$ at such times, a situation that displays the monogamy behaviour of entanglement: when MBSs and the right QD are maximally entangled, the right QD cannot be entangled with the left QD, thus leading to $C = 0$. Interestingly, the vanishing concurrence of the MS ($C = 0$) is accompanied by vanishing discord ($D = 0$), which reveals the absence of quantum correlations and that the system transitions into a classical state, an effect only obtained in the MS but not in the NFS, see Fig. 3(a,b). To further visualize the achieved entanglement between MBSs and right QD, in Fig. 3(c) we schematically illustrate the entanglement shift that corresponds to the two times of the evolution indicated by red and magenta stars in Fig. 3(a). This entanglement shift reveals the possibility of starting with two maximally entangled QDs and then generate maximally entanglement between MBSs and right QD during the time evolution. In contrast to the MS system,

the entanglement measures for the NFS develop a profile where it is not simple to determine the generation maximal entanglement between MBSs and QDs, Fig. 3(b); their evolution is similar to Fig. 2(b,d,f,h). Therefore, it is possible to induce maximally entangled states between MBSs and QDs, even though for this purpose finite energy MBSs are needed, which, however, are not nonlocal and might not serve the purpose of encoding information nonlocally.

IV. RESULTS FOR A SEPARABLE INITIAL STATE

Having studied the state dynamics and quantum correlations for a maximally entangled initial state, in this section we focus on the same quantities but taking an initial state that is completely separable in both systems, the MS and NFS. Thus, using the same notation as before, we consider the initial state to be given by

$$|\psi(0)\rangle = |110\rangle, \quad (27)$$

which represents a separable state because it can be written as $|110\rangle = |1\rangle|1\rangle|0\rangle$. This state has excitations in the two QDs, but the nonlocal fermion (or normal fermion when dealing with the NFS) is in the $|0\rangle$ state. We note that this separable state is also realistic because the two QDs can be initially prepared to be occupied, with a vanishing coupling to the topological superconductor controlled by voltage gates [56–58], see also Refs. [54, 55]. Moreover, we consider the $|0\rangle$ state of the nonlocal fermion because it preserves the even parity of the system. To maintain consistency with the initial state of Section III and our findings therein, here we do not consider the other two separable states, $|011\rangle$ and $|101\rangle$, because they require the nonlocal fermion (or local fermion in the NFS) in the $|1\rangle$ state. Furthermore, we do not address state $|000\rangle$ because this state becomes an eigenstate for the NFS, implying that the state will evolve with a constant phase which does not affect the entanglement measures over time. The desired state for obtaining the entanglement dynamics using Eq. (15) is also taken to be the same as in Eq. (20). For the separable initial state, the expressions of the entanglement measures for the MS and NFS cannot be expressed in a simplified form. Nevertheless, we list the time-dependent coefficients of the time evolved states which are required for obtaining quantum correlations and state dynamics, as discussed in Section III.

We calculate the time evolution of the $|110\rangle$ state for the MS and NFS systems, which can be written in a similar form as $|\psi(t)\rangle$ in Eq. (24). The coefficients of

evolution for the MS are given by

$$\begin{aligned} c_{1(4)}(t) &= \frac{1}{2} \left\{ \left[\cos \Delta t + i \frac{\omega}{\Delta} \sin \Delta t \right] \right. \\ &\quad \mp \left[\cos \Delta_1 t + i \frac{\omega}{\Delta_1} \sin \Delta_1 t \right] \left. \right\}, \\ c_{2(3)}(t) &= \frac{i}{2} \left\{ \frac{-(\lambda - 1)}{\Delta} \sin \Delta t \right. \\ &\quad \left. \pm \frac{(\lambda + 1)}{\Delta_1} \sin \Delta_1 t \right\}, \end{aligned} \quad (28)$$

while for the NFS we obtain

$$\begin{aligned} \bar{c}_1'(t) &= 0, \\ \bar{c}_2'(t) &= \frac{1}{2\sqrt{1 + \lambda^2 + \omega^2}} (e^{-i\Delta_- t} - e^{-i\Delta_+ t}), \\ \bar{c}_3'(t) &= \frac{-\lambda}{2\sqrt{1 + \lambda^2 + \omega^2}} (e^{-i\Delta_- t} - e^{-i\Delta_+ t}), \\ \bar{c}_4'(t) &= \frac{1}{2\sqrt{1 + \lambda^2 + \omega^2}} (\Delta_+ e^{-i\Delta_- t} - \Delta_- e^{-i\Delta_+ t}), \end{aligned} \quad (29)$$

where λ characterizes the coupling to the right QD, ω is the energy of MBSs (normal fermion), Δ , Δ_1 , and Δ_{pm} are given below Eqs. (3) and Eqs. (6). It is important to note that all the coefficients for MS setup are finite and hence a complex time evolution is expected. Moreover, contrary to the coefficients of $|\psi(t)\rangle$ for initially maximally entangled states of the QDs in Eq. (25) for NFS, the first coefficient, $\bar{c}_1'(t)$, goes to zero. This occurs because the state $|000\rangle$ is an eigenstate of the system, and the initial state does not contain the configuration $|000\rangle$. Therefore, it does not contribute to the evolution (see Eq. (17)). The other coefficients are non-zero and show a similar form of dependence on λ and ω , as we will observe in the dynamics. Using the coefficients from Eq. (28) and Eq. (29) for MS and NFS, and following the steps to calculate the state dynamical function and quantum correlations given in Section III, we obtain E_d , C , and D and discuss their time evolution next.

A. Discussion of the state dynamics and quantum correlations

After obtaining the entanglement measures for a separable initial state, we plot them in Fig. 4 as a function of time for symmetric and asymmetric couplings between QDs and MBSs (normal fermion) in the MS (NFS) setup. To inspect the nonlocal nature of MBSs, we consider $\omega = 0$ and also $\omega \neq 0$ in the two cases and for the two systems.

In the case of symmetric couplings ($\lambda = 1$), the immediate observation is that almost all the quantities oscillate with time, with different patterns at $\omega = 0$ and $\omega \neq 0$, which is different to what we observed in the previous section for initial maximally entangled QDs. For the MS case in Fig. 4(a), the quantities R_p , E_d , and D oscillate, while $C = 0$, implying that the completely nonlocal

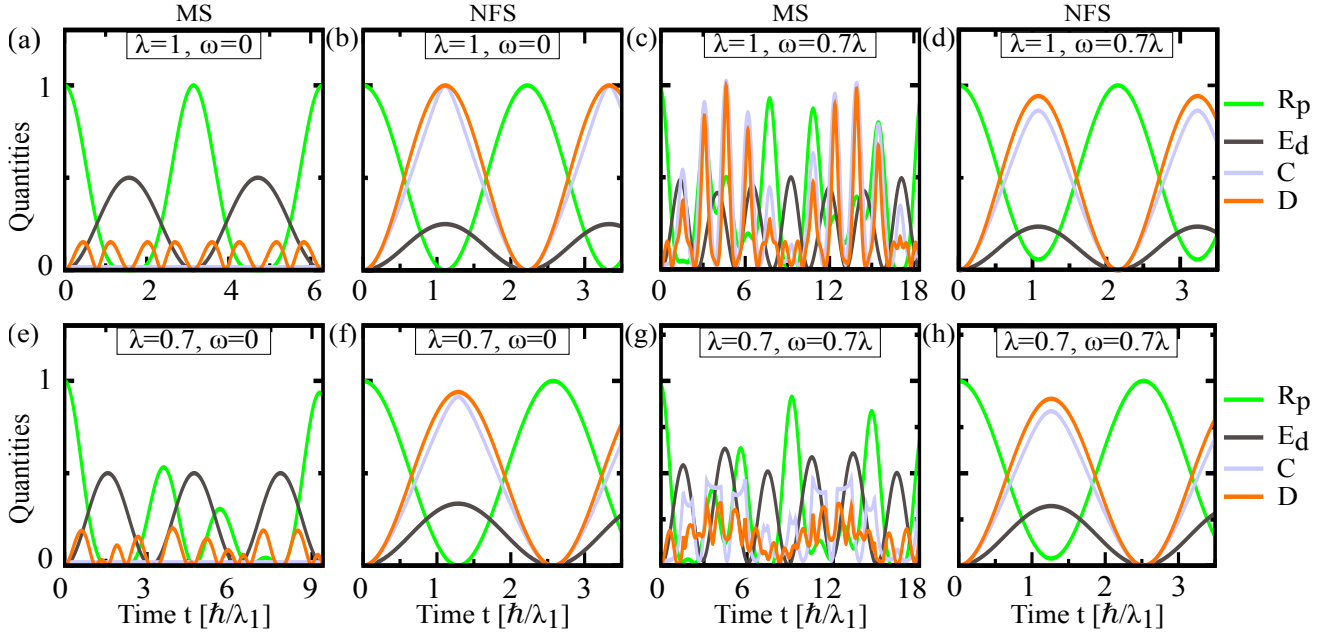


FIG. 4. Time evolution of concurrence, discord, return probability, and entanglement dynamics, denoted by C , D , R_p , and E_d , with a separable initial state for MS and NFS. (a, b) at $\lambda = 1$ and $\omega = 0$; (c, d) at $\lambda = 1$ and $\omega \neq 0$; (e, f) at $\lambda \neq 1$ and $\omega = 0$; and (g, h) at $\lambda \neq 1$ and $\omega \neq 0$.

zero-energy MBSs cannot generate entanglement in this case. For the entanglement dynamics and return probability, we obtain $E_d = \sin^2 t$ and $R_p = \cos^2 t$, which, at $t = (\pi/2) \hbar/\lambda_1$, become $E_d = 0.5$ and $R_p = 0$, as depicted by black and green curves in Fig. 4(a). By obtaining $c_1(t) = 1$, we conclude that at those points in time, the state $|000\rangle$ is present. In relation to the discord D in Fig. 4(a), it exhibits homogeneous oscillations as a function of time, with period equal to $T = (\pi/4) \hbar/\lambda_1$, acquiring vanishing values at points where C vanishes, a phenomenon we have seen to occur only for MS in Figs. 2 and Fig. 3 of the previous section. The times at which the discord completes a period $(\pi/4)$ are special because the eigenvalues of the marginal entropies are $\{0, 1\}$ at $\theta = \pi/4$ and $\phi = \pi/4$, which then gives vanishing conditional entropy when obtaining the discord in Eq. 13, see also Eq. (A7) and Eq. (A8) in Appendix A 1. Moreover, the composite entropy and the single QD entropy are the same and equal to unity, thus the total algebraic sum goes to zero, see details in Eq. (A8) in Appendix A 1. When analyzing the time $t = (\pi/2) \hbar/\lambda_1$, we have $c_1(t) = 1$ in Eq. (28) which gives a pure state description, where all entropies go to zero. For a finite overlap ($\lambda = 1, \omega = 0.7$), plotted in Fig. 4(c), an extra frequency in oscillation is introduced because of ω . The entanglement is generated between QDs with fast and slow frequencies. In this case, C and D reach unity simultaneously, implying that maximum quantum correlation can be created by MBSs at finite energy splitting [62]. We conclude that, while quantum correlations can be generated with zero-energy MBSs but they remain small, entanglement generation is possible only with a finite energy splitting of MBSs.

For asymmetric couplings at $\lambda = 0.7$, the situation is slightly different but with some similarities, see Fig. 4(e,g) for $\omega = 0$ and $\omega \neq 0$ in the MS setup. First of all, R_p , E_d , and D oscillate with time, see Fig. 4(e,g). As for the symmetric case, $C = 0$ throughout the evolution at $\omega = 0$ [Fig. 4(e)], meaning that entanglement can not be generated. This is because the eigenenergies in Eqs. (4) are given by $\Delta = |\lambda - 1|$, which simplifies the coefficients in Eq. (28) as $c_{1(4)}(t) = [\cos(\lambda - 1)t \mp \cos(\lambda + 1)t]/2$, $c_{2(3)}(t) = \pm i[\sin(\lambda + 1)t \mp \sin(\lambda - 1)t]/2$. This gives $|c_1(t)||c_4(t)| = |c_2(t)||c_3(t)| = |\sin^2(\lambda - 1)t - \sin^2(\lambda + 1)t|$. Therefore, the concurrence C , as defined in Eq. (26), goes to zero throughout the evolution, see Fig. 4(e). However, at $\omega \neq 0$, C takes finite values and develops an oscillatory profile, see Fig. 4(g). In relation to the discord, it develops oscillations with different periodicities, acquiring a beating profile that oscillates faster for finite frequencies, as seen in Fig. 4(e,g). We note that the complex behaviour of D stems from the fact that it is determined by different entropies, see Appendix A 1. When it comes to the entanglement dynamics in asymmetric couplings ($\lambda \neq 1$) with $\omega = 0$, we find that $E_d = \sin^2 t/2$ which is independent of λ and has a constant period of π as seen Fig. 4(e). In contrast, in the same regime, we obtain the return probability to be $R_p = \cos^2 \lambda t \cos^2 t$, which clearly depends on two periods, π/λ and π . Therefore, the system takes a long time to return to the initial state, beyond the scope of Fig. 4(e). For clarification, we note that the first maxima of R_p happens at $t = (10\pi) \hbar/\lambda_1$. Moving into the asymmetric couplings ($\lambda \neq 1$) and finite $\omega \neq 0$, as shown in Fig. 4(g), the quantities R_p , E_d , C , and D exhibit an oscillatory dynamics

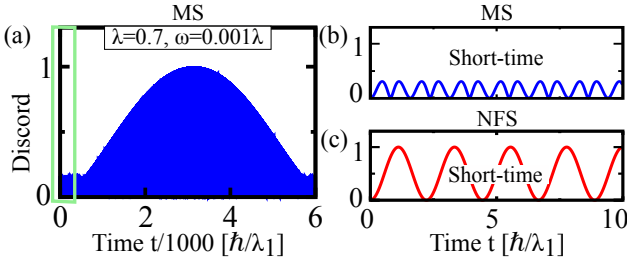


FIG. 5. Time evolution of discord at $\lambda = 0.7$ and $\omega = 0.001\lambda$ for a MS (a,b) and a NFS (c). Panel (a) shows the long-time evolution, while (b,c) shows the short-time behaviour. The short times for the MS in (b) are indicated by the green box in (a). We note that, for these parameters, the long-time evolution of discord for the NFS has the same behaviour as the short-time counterpart in (c).

without showing any special entanglement characteristics, unlike their counterparts for a maximally entangled initial state discussed in Section III.

In relation to the entanglement measures for the NFS system, shown in Fig. 4(b,d,f,h), they exhibit a behaviour that is roughly similar either at finite or zero energies and at symmetric or asymmetric couplings. Here, the concurrence we obtain to be equal to $C = ||\tilde{c}_2(t)||||\tilde{c}_3(t)||$, which goes to zero when either of the coefficients approaches zero. The time at which $C = 0$ is calculated as $t = (n\pi/\sqrt{1 + \lambda^2 + \omega^2}) \hbar/\lambda_1$, where n is an integer. At these points in time, the NFS acquires the state $|110\rangle$, which is a zero concurrence state ($C = 0$). This can be verified from the results in Fig. 4(b,d,f,h), where zero concurrence occurs between $t = 2 \hbar/\lambda_1$ and $t = 3 \hbar/\lambda_1$, depending on the particular value of λ and ω during the evolution.

B. Generating maximally entangled QDs induced by MBSs

We have seen in the previous subsection that the time-evolution in the MS setup is sensitive to variations of ω . Of particular interest in this part is the behaviour of the quantum correlations at $\omega \sim 0$, because this regime has well localized MBSs in the MS. Here we exploit the sensitivity of discord D at $\omega \sim 0$ to generate a maximally entangled state between QDs. The time evolution of D at $\omega = 0.001$ and asymmetric coupling $\lambda = 0.7$ is presented in Fig. 5(a,b) for the MS setup for long and short times, with Fig. 5(b) taken within the green box Fig. 5(a). We contrast this behavior with the time evolution for the NFS at short times. The first observation is that D exhibits rapid oscillations with an initial small amplitude of 0.1 at short times [Fig. 5(b)]. As time progresses, D increases and eventually reaches unity in the long-term evolution, see Fig. 5(a). Having $D = 1$ means that a maximally entangled state of QDs is created, achieved only at a small energy splitting of MBSs. In contrast to the MS, the discord for the NFS system in Fig. 5(c)

develops homogeneous oscillations at short times whose period and amplitudes do not change over time. We have verified that this behaviour in the NFS also remains in the long time dynamics, making it very different to the MS.

V. CONCLUSIONS

In conclusion, we have investigated the entanglement properties of Majorana bound states emerging in a topological superconductor that is coupled to two quantum dots. To contrast the impact of Majorana bound states, we have compared this Majorana system with an equivalent where the quantum dots are coupled via a normal fermion. In order to characterize entanglement in both systems, we have employed the concurrence and discord, quantum correlations that we also complemented by studying the entanglement dynamics and return probability. We found that zero-energy Majorana bound states can transform initially maximally entangled quantum dots into a classical state, while maximally entangled states are notably achieved at finite Majorana energies, thus highlighting the impact of Majorana nonlocality. Remarkably, we have shown that the maximal entanglement between quantum dots at the beginning of the evolution can be completely shift to a state between Majorana bound states and one of the quantum dots.

Furthermore, we found entanglement and quantum correlations can be generated from an initially separable state in the Majorana system, with discord reliably quantifying quantum correlations for zero-energy Majorana bound states. We also showed that entanglement generation in the Majorana system is very sensitive to the nonlocality of the Majorana bound states, which, upon an appropriate control, can even induce maximally entangled states in the long time dynamics. In all the studied cases, we found that the Majorana system exhibits distinct entanglement features than the normal fermion system, which occurs because spatial nonlocality is intrinsic to Majorana bound states but absent in regular fermions. Our findings can therefore serve as an alternative way to characterize Majorana bound states and exploit their potential for quantum information.

VI. ACKNOWLEDGEMENTS

We thank J. C. Abadillo-Uriel, M. Benito, V. A. Mousolou, and E. Sjöqvist for insightful discussions. We acknowledge financial support from the Swedish Research Council (Vetenskapsrådet Grant No. 2021-04121) and from the Carl Trygger's Foundation (Grant No. 22:2093).

Appendix A: Calculation of quantum discord

In this Appendix, we outline the procedure for computing quantum discord [44] as defined in the main text for both MS and NFS. Here, for the comparative study of concurrence, we focus on the quantum discord between the two QDs, which can be calculated using the two-qubit reduced density matrix ρ_d defined in Eq. (10) for both systems. We provide the procedure to compute discord for MS first, followed by that for NFS in the subsequent subsection.

1. Majorana system

For initially maximally entangled QDs in the MS, the matrix ρ_d in Eq. (10) is computed by tracing over the nonlocal fermion from the state described in Eq. (18). On the other hand, for the separable initial state of the MS written in Eq. (27), the same can be calculated from the state formulated by Eq. (28). In both scenarios, the resulting ρ_d matrices represent the reduced density matrix of the two QDs. Therefore, the basis states and the form of matrices remain unchanged. Subsequently, for a better representation, the first QD is denoted as subsystem A and the second QD as subsystem B. Therefore, ρ_d for the two QDs will be denoted as ρ_{AB} and will have the same X -state representation as written in Eq. (10). For the discord calculation, we set the measurement basis of B as $\{|\tilde{0}\rangle, |\tilde{1}\rangle\}$, parametrized by θ and ϕ , which can be transformed from the computational basis $\{|0\rangle, |1\rangle\}$ of B as

$$\begin{aligned} |\tilde{0}\rangle &= \cos \theta/2 |0\rangle + e^{i\phi} \sin \theta/2 |1\rangle, \\ |\tilde{1}\rangle &= \sin \theta/2 |0\rangle - e^{i\phi} \cos \theta/2 |1\rangle, \end{aligned} \quad (\text{A1})$$

where the parameters $\theta \in [0, \pi]$ and $\phi \in [0, 2\pi]$. In the new basis states $\{|\tilde{k}\rangle\} = \{|\tilde{0}\rangle, |\tilde{1}\rangle\}$, we compute the marginal conditional density matrices $\rho_{A|B_{\tilde{k}}}$ to obtain the conditional entropy in Eq. (13) as

$$\rho_{A|B_{\tilde{k}}} = \frac{1}{p_{\tilde{k}}} \text{Tr}_B |\tilde{k}\rangle \langle \tilde{k}| \rho_{AB}, \quad p_{\tilde{k}} = \text{Tr}_{AB} |\tilde{k}\rangle \langle \tilde{k}| \rho_{AB}, \quad (\text{A2})$$

where the expressions for the probabilities $p_{\tilde{k}}$ are obtained using the element of ρ_{AB} , borrowed from Eq. (10) as

$$\begin{aligned} p_{\tilde{0}} &= (u + w_2) \cos^2(\theta/2) + (v + w_1) \sin^2(\theta/2), \\ p_{\tilde{1}} &= (u + w_2) \sin^2(\theta/2) + (v + w_1) \cos^2(\theta/2). \end{aligned} \quad (\text{A3})$$

Therefore, the eigenvalues of $\rho_{A|B_{\tilde{k}}}$ in terms of the above probabilities can be calculated as

$$\begin{aligned} \lambda_{\pm} &= \frac{1}{2p_{\tilde{0}}} (p_{\tilde{0}} \pm \sqrt{b_{\tilde{0}}^2 + 4|z|^2}), \quad \text{for } \rho_{A|B_{\tilde{0}}}, \\ \lambda'_{\pm} &= \frac{1}{2p_{\tilde{1}}} (p_{\tilde{1}} \pm \sqrt{b_{\tilde{1}}^2 + 4|z|^2}), \quad \text{for } \rho_{A|B_{\tilde{1}}}, \end{aligned} \quad (\text{A4})$$

where, $z = \frac{1}{2} \sin \theta (e^{i\phi} x + e^{-i\phi} y)$ and

$$\begin{aligned} b_{\tilde{0}} &= (u - w_2) \cos^2(\theta/2) + (w_1 - v) \sin^2(\theta/2), \\ b_{\tilde{1}} &= (u - w_2) \sin^2(\theta/2) + (w_1 - v) \cos^2(\theta/2). \end{aligned} \quad (\text{A5})$$

Using all the expressions from Eq. (A3-A5), the conditional entropy $C_{\theta, \phi}(\rho_{A|B_{\tilde{k}}})$ can be written by the weighted sum of marginal conditional entropies as

$$C_{\theta, \phi}(\rho_{A|B}) = p_{\tilde{0}} S(\rho_{A|B_{\tilde{0}}}) + p_{\tilde{1}} S(\rho_{A|B_{\tilde{1}}}), \quad (\text{A6})$$

where the marginal entropies are computed using the eigenvalues written in Eq. (A4) as follows

$$\begin{aligned} S(\rho_{A|B_{\tilde{0}}}) &= -\lambda_+ \log_2 \lambda_+ - \lambda_- \log_2 \lambda_-, \\ S(\rho_{A|B_{\tilde{1}}}) &= -\lambda'_+ \log_2 \lambda'_+ - \lambda'_- \log_2 \lambda'_-. \end{aligned} \quad (\text{A7})$$

Now, we can compute the quantum discord of the two QDs as defined in Eq. (14) as

$$D_{AB} = \min_{(\theta, \phi)} C_{\theta, \phi}(\rho_{A|B}) - S(\rho_{AB}) + S(\rho_B), \quad (\text{A8})$$

where the conditional entropy $C_{\theta, \phi}(\rho_{A|B})$ is given by Eq. (A6) and can be minimized computationally over the angles θ and ϕ . The composite entropy $S(\rho_{AB})$ is calculated using the eigenvalues of the ρ_{AB} borrowed from Eq. (10), which are $(u + v \pm \sqrt{(u - v)^2 + 4|y|^2})/2$ and $(w_1 + w_2 \pm \sqrt{(w_1 - w_2)^2 + 4|x|^2})/2$. The last term, $S(\rho_B)$, represents the entropy of the second QD. Here, the matrix ρ_B is obtained from ρ_{AB} by tracing over A. The entropy $S(\rho_B)$ is then calculated using the eigenvalues $u + w_2$ and $v + w_1$ of ρ_B . Therefore, Eq. (A8) can be used to calculate the discord in Eq. (14) for the MS with different initial states written in Eq. (18) and Eq. (28) by first computing ρ_d s as described in Eq. (10) and following the steps to Eq. (A8) of this section. These calculations have been utilized in Sec. III and Sec. IV.

2. Normal fermion system

The computation of discord for NFS follows the same steps as for MS. However, for NFS, the reduced density matrix ρ_d for the two QDs is obtained by tracing over the normal fermion, as described in Eq. (8), from the state given in Eq. (24) for the maximally entangled initial state. Alternatively, for the separable initial state, ρ_d can be calculated from the state in Eq. (29). Then, similar to the MS in previous subsection, we use ρ_{AB} for the reduced density matrices of the two QDs and follow the steps from equations (A1) to (A8) to compute all the relevant quantities. The minimization of the conditional entropy in Eq. (A8) is carried out numerically. Therefore, we directly refer to Eq. (A8) for computing the discord between the two QDs in NFS. The difference in discord from MS to NFS lies in the initial states used: Eq. (24) and Eq. (29) for the maximally entangled and separable initial states of NFS, respectively. We utilize these calculations in Sections III and IV for NFS.

-
- [1] Y. Tanaka, M. Sato, and N. Nagaosa, Symmetry and topology in superconductors—odd-frequency pairing and edge states—, *J. Phys. Soc. Japan* **81**, 011013 (2012).
- [2] M. Sato and Y. Ando, Topological superconductors: A review, *Rep. Prog. Phys.* **80**, 076501 (2017).
- [3] R. Aguado, Majorana quasiparticles in condensed matter, *Riv. Nuovo Cimento* **40**, 523 (2017).
- [4] R. M. Lutchyn, E. P. Bakkers, L. P. Kouwenhoven, P. Krogstrup, C. M. Marcus, and Y. Oreg, Majorana zero modes in superconductor–semiconductor heterostructures, *Nat. Rev. Mater.* **3**, 52 (2018).
- [5] S. M. Frolov, M. J. Manfra, and J. D. Sau, Topological superconductivity in hybrid devices, *Nat. Phys.* **16**, 718 (2020).
- [6] H. Zhang, D. E. Liu, M. Wimmer, and L. P. Kouwenhoven, Next steps of quantum transport in Majorana nanowire devices, *Nat. Commun.* **10**, 5128 (2019).
- [7] E. Prada, P. San-Jose, M. W. de Moor, A. Geresdi, E. J. Lee, J. Klinovaja, D. Loss, J. Nygård, R. Aguado, and L. P. Kouwenhoven, From Andreev to Majorana bound states in hybrid superconductor–semiconductor nanowires, *Nat. Rev. Phys.* **2**, 575 (2020).
- [8] K. Flensberg, F. von Oppen, and A. Stern, Engineered platforms for topological superconductivity and Majorana zero modes, *Nat. Rev. Mater.* **6**, 944 (2021).
- [9] Y. Tanaka, S. Tamura, and J. Cayao, Theory of Majorana zero modes in unconventional superconductors, arXiv:2402.00643 (2024).
- [10] S. D. Sarma, M. Freedman, and C. Nayak, Majorana zero modes and topological quantum computation, *npj Quantum Inf.* **1**, 15001 (2015).
- [11] V. Lahtinen and J. K. Pachos, A Short Introduction to Topological Quantum Computation, *SciPost Phys.* **3**, 021 (2017).
- [12] C. W. J. Beenakker, Search for non-Abelian Majorana braiding statistics in superconductors, *SciPost Phys. Lect. Notes*, 15 (2020).
- [13] R. Aguado and L. P. Kouwenhoven, Majorana qubits for topological quantum computing, *Physics Today* **73**, 44 (2020).
- [14] P. Marra, Majorana nanowires for topological quantum computation, *J. Appl. Phys.* **132**, 231101 (2022).
- [15] D. Bagrets and A. Altland, Class *D* spectral peak in Majorana quantum wires, *Phys. Rev. Lett.* **109**, 227005 (2012).
- [16] D. I. Pikulin, J. P. Dahlhaus, M. Wimmer, H. Schomerus, and C. W. J. Beenakker, A zero-voltage conductance peak from weak antilocalization in a Majorana nanowire, *New J. Phys.* **14**, 125011 (2012).
- [17] G. Kells, D. Meidan, and P. W. Brouwer, Near-zero-energy end states in topologically trivial spin-orbit coupled superconducting nanowires with a smooth confinement, *Phys. Rev. B* **86**, 100503 (2012).
- [18] E. Prada, P. San-Jose, and R. Aguado, Transport spectroscopy of *ns* nanowire junctions with Majorana fermions, *Phys. Rev. B* **86**, 180503 (2012).
- [19] J. Cayao, E. Prada, P. San-Jose, and R. Aguado, SNS junctions in nanowires with spin-orbit coupling: Role of confinement and helicity on the subgap spectrum, *Phys. Rev. B* **91**, 024514 (2015).
- [20] C. Reeg, O. Dmytruk, D. Chevallier, D. Loss, and J. Klinovaja, Zero-energy Andreev bound states from quantum dots in proximitized Rashba nanowires, *Phys. Rev. B* **98**, 245407 (2018).
- [21] O. A. Awoga, J. Cayao, and A. M. Black-Schaffer, Supercurrent detection of topologically trivial zero-energy states in nanowire junctions, *Phys. Rev. Lett.* **123**, 117001 (2019).
- [22] P. Marra and M. Nitta, Topologically nontrivial Andreev bound states, *Phys. Rev. B* **100**, 220502 (2019).
- [23] O. Dmytruk, D. Loss, and J. Klinovaja, Pinning of Andreev bound states to zero energy in two-dimensional superconductor–semiconductor Rashba heterostructures, *Phys. Rev. B* **102**, 245431 (2020).
- [24] S. Das Sarma and H. Pan, Disorder-induced zero-bias peaks in Majorana nanowires, *Phys. Rev. B* **103**, 195158 (2021).
- [25] J. Cayao and P. Buset, Confinement-induced zero-bias peaks in conventional superconductor hybrids, *Phys. Rev. B* **104**, 134507 (2021).
- [26] B. S. de Mendonça, A. L. R. Manesco, N. Sandler, and L. G. G. V. Dias da Silva, Near zero energy caroli–de gennes–matricon vortex states in the presence of impurities, *Phys. Rev. B* **107**, 184509 (2023).
- [27] O. A. Awoga, M. Leijnse, A. M. Black-Schaffer, and J. Cayao, Mitigating disorder-induced zero-energy states in weakly coupled superconductor–semiconductor hybrid systems, *Phys. Rev. B* **107**, 184519 (2023).
- [28] X.-F. Chen, W. Luo, T.-F. Fang, Y. Paltiel, O. Millo, A.-M. Guo, and Q.-F. Sun, Topologically nontrivial and trivial zero modes in chiral molecules, *Phys. Rev. B* **108**, 035401 (2023).
- [29] S. Das Sarma, J. D. Sau, and T. D. Stanescu, Splitting of the zero-bias conductance peak as smoking gun evidence for the existence of the Majorana mode in a superconductor–semiconductor nanowire, *Phys. Rev. B* **86**, 220506 (2012).
- [30] D. Rainis, L. Trifunovic, J. Klinovaja, and D. Loss, Towards a realistic transport modeling in a superconducting nanowire with Majorana fermions, *Phys. Rev. B* **87**, 024515 (2013).
- [31] J. Cayao, P. San-Jose, A. M. Black-Schaffer, R. Aguado, and E. Prada, Majorana splitting from critical currents in Josephson junctions, *Phys. Rev. B* **96**, 205425 (2017).
- [32] J. Ulrich and F. Hassler, Majorana-assisted nonlocal electron transport through a floating topological superconductor, *Phys. Rev. B* **92**, 075443 (2015).
- [33] J. Cayao and A. M. Black-Schaffer, Finite length effect on supercurrents between trivial and topological superconductors, *Eur. Phys. J.: Spec. Top.* **227**, 1387 (2018).
- [34] M.-T. Deng, S. Vaitiekėnas, E. Prada, P. San-Jose, J. Nygård, P. Krogstrup, R. Aguado, and C. M. Marcus, Nonlocality of Majorana modes in hybrid nanowires, *Phys. Rev. B* **98**, 085125 (2018).
- [35] J. Cayao and A. M. Black-Schaffer, Distinguishing trivial and topological zero-energy states in long nanowire junctions, *Phys. Rev. B* **104**, L020501 (2021).
- [36] L. Baldo, L. G. D. Da Silva, A. M. Black-Schaffer, and J. Cayao, Zero-frequency supercurrent susceptibility signatures of trivial and topological zero-energy states in nanowire junctions, *Supercond. Sci. Technol.* **36**, 034003 (2023).

- (2023).
- [37] M. Thamm and B. Rosenow, Machine learning optimization of Majorana hybrid nanowires, *Phys. Rev. Lett.* **130**, 116202 (2023).
 - [38] J. Cayao, P. Dutta, P. Burset, and A. M. Black-Schaffer, Phase-tunable electron transport assisted by odd-frequency cooper pairs in topological Josephson junctions, *Phys. Rev. B* **106**, L100502 (2022).
 - [39] P. Dutta, J. Cayao, A. M. Black-Schaffer, and P. Burset, Nonlocality of Majorana bound states revealed by electron waiting times in a topological Andreev interferometer, *Phys. Rev. Res.* **6**, L012062 (2024).
 - [40] A. Kejriwal and B. Muralidharan, Nonlocal conductance and the detection of Majorana zero modes: Insights from von Neumann entropy, *Phys. Rev. B* **105**, L161403 (2022).
 - [41] M. A. Nielsen and I. L. Chuang, *Quantum Computation and Quantum Information: 10th Anniversary Edition* (Cambridge University Press, 2011).
 - [42] W. K. Wootters, Entanglement of formation of an arbitrary state of two qubits, *Phys. Rev. Lett.* **80**, 2245 (1998).
 - [43] V. K. Vimal and V. Subrahmanyam, Quantum correlations and entanglement in a Kitaev-type spin chain, *Phys. Rev. A* **98**, 052303 (2018).
 - [44] V. Kumar Vimal and V. Subrahmanyam, Magnetization revivals and dynamics of quantum correlations in a Kitaev spin chain, *Phys. Rev. A* **102**, 012406 (2020).
 - [45] A. Datta, A. Shaji, and C. M. Caves, Quantum discord and the power of one qubit, *Phys. Rev. Lett.* **100**, 050502 (2008).
 - [46] B. P. Lanyon, M. Barbieri, M. P. Almeida, and A. G. White, Experimental quantum computing without entanglement, *Phys. Rev. Lett.* **101**, 200501 (2008).
 - [47] B. Dakić, Y. O. Lipp, X. Ma, M. Ringbauer, S. Kropatschek, S. Barz, T. Paterek, V. Vedral, A. Zeilinger, v. Brukner, and P. Walther, Quantum discord as resource for remote state preparation, *Nature Phys* **8**, 666 (2012).
 - [48] A. Brodutch, Discord and quantum computational resources, *Phys. Rev. A* **88**, 022307 (2013).
 - [49] S. Pirandola, Quantum discord as a resource for quantum cryptography, *Sci. Rep.* **4**, 6956 (2014).
 - [50] M. P. Almeida, M. Gu, A. Fedrizzi, M. A. Broome, T. C. Ralph, and A. G. White, Entanglement-free certification of entangling gates, *Phys. Rev. A* **89**, 042323 (2014).
 - [51] H. A. Mansour, F.-Z. Siyouri, M. Faqir, and M. E. Baz, Quantum correlations dynamics in two coupled semiconductor inas quantum dots, *Phys. Scr.* **95**, 095101 (2020).
 - [52] H. Ait Mansour, M. Faqir, and M. El Baz, Global quantum discord and entanglement in two coupled double quantum dots AlGaAs/GaAs, *Int J Theor Phys* **62**, 58 (2023).
 - [53] H. Ollivier and W. H. Zurek, Quantum discord: A measure of the quantumness of correlations, *Phys. Rev. Lett.* **88**, 017901 (2001).
 - [54] W. G. van der Wiel, S. De Franceschi, J. M. Elzerman, T. Fujisawa, S. Tarucha, and L. P. Kouwenhoven, Electron transport through double quantum dots, *Rev. Mod. Phys.* **75**, 1 (2002).
 - [55] S. De Franceschi, L. Kouwenhoven, C. Schönenberger, and W. Wernsdorfer, Hybrid superconductor–quantum dot devices, *Nat. Nanotech.* **5**, 703 (2010).
 - [56] T. Dvir, G. Wang, N. van Loo, C.-X. Liu, G. P. Mazur, A. Bordin, S. L. D. ten Haaf, J.-Y. Wang, D. van Driel, F. Zatelli, X. Li, F. K. Malinowski, S. Gazibegovic, G. Badawy, E. P. A. M. Bakkers, M. Wimmer, and L. P. Kouwenhoven, Realization of a minimal Kitaev chain in coupled quantum dots, *Nature* **614**, 445 (2023).
 - [57] A. Bordin, G. Wang, C.-X. Liu, S. L. D. ten Haaf, N. van Loo, G. P. Mazur, D. Xu, D. van Driel, F. Zatelli, S. Gazibegovic, G. Badawy, E. P. A. M. Bakkers, M. Wimmer, L. P. Kouwenhoven, and T. Dvir, Tunable crossed Andreev reflection and elastic cotunneling in hybrid nanowires, *Phys. Rev. X* **13**, 031031 (2023).
 - [58] A. Bordin, X. Li, D. van Driel, J. C. Wolff, Q. Wang, S. L. D. ten Haaf, G. Wang, N. van Loo, L. P. Kouwenhoven, and T. Dvir, Crossed Andreev reflection and elastic co-tunneling in a three-site Kitaev chain nanowire device, arXiv:2306.07696 (2023).
 - [59] B. M. Terhal, Is entanglement monogamous?, *IBM Journal of Research and Development* **48**, 71 (2004).
 - [60] At $t = (\pi/\sqrt{2}) \hbar/\lambda_1$, the coefficients $\bar{c}_2(t)$ and $\bar{c}_3(t)$ are zero and $\bar{c}_4(t) = -1$; therefore, the state of the system becomes $(|000\rangle - |110\rangle)/2$, which is also a maximally entangled state of the QDs, thus giving $C = 1$.
 - [61] We have verified that the revival of the initial state occurs over a longer period of time than shown in the plot.
 - [62] J. Li, T. Yu, H.-Q. Lin, and J. Q. You, Probing the non-locality of Majorana fermions via quantum correlations, *Sci. Rep.* **4**, 4930 (2014).